Available online at www.sciencedirect.com
ScienceDirect
Ceramics International 35 (2009) 1335–1343
CERAMICS INTERNATIONAL
www.elsevier.com/locate/ceramint

Synthesis and electrical properties of $Ce_{0.8}Sm_{0.2}O_{1.9}$ ceramics for IT-SOFC electrolytes by urea-combustion technique

Min Chen [a], Bok Hee Kim [a,*], Qing Xu [b,**], Byeong Kuk Ahn [a], Woo Jin Kang [a], Duan ping Huang [b]

[a] *Department of Hydrogen and Fuel cells Engineering, Hydrogen & Fuel Cell Research Center, Chonbuk National University, 1-664-14, Duckjin-dong, Duckjin-ku, Jeonju, Jeonbuk 561-756, South Korea*
[b] *School of Materials Science and Engineering, Wuhan University of Technology, Wuhan 430070, PR China*

Received 28 January 2008; received in revised form 20 May 2008; accepted 20 June 2008
Available online 22 July 2008

Abstract

Fine $Ce_{0.8}Sm_{0.2}O_{1.9}$ (SDC) powders with a fluorite cubic phase were prepared using a urea-combustion technique. The sinterability and microstructural evolution of the resulting ceramics were investigated. The results indicate that the ceramics sintered above 1350 °C display relative densities of about 98.5% along with significant grain growth. With respect to their electrical conduction properties, the specimens sintered above 1350 °C exhibit an excellent total ionic conductivity of 0.082 S cm^{-1} at 800 °C in air. However, when measured in an N_2 + 33.3%H_2 atmosphere, a pronounced Warburg feature appears in the impedance plots of the SDC ceramics, together with a significant increase of the total conductivity at measuring temperatures above 550 °C, due to the introduction of a mixed Ce^{4+}/Ce^{3+} valence state and the generation of the electronic conduction in the reducing atmosphere.

Keywords: A. Powders: chemical preparation; B. Grain boundaries; C. Ionic conductivity; E. Fuel cells

1. Introduction

Nowadays, Ceria-based solid solutions have been considered as promising electrolytes for intermediate temperature (600–800 °C) solid oxide fuel cells (IT-SOFCs) due to their excellent oxygen-ion conductivity compared to yttria-stabilized zirconia (YSZ). The oxygen-ion conductivities of ceria-based electrolytes, doped with various ions (e.g., Sr^{2+}, Ca^{2+}, Y^{3+}, La^{3+}, Gd^{3+} and Sm^{3+}) at different concentrations have been extensively studied [1–4]. Among them, Sm^{3+} doped CeO_2 was found to exhibit the highest oxygen-ion conductivity at certain fixed doping levels, because of its having the smallest association enthalpy between the dopant cations and oxygen vacancies in the fluorite lattice [5,6].

Solid electrolytes for SOFCs should be highly dense to avoid direct reaction between the fuel at the anode and oxygen at the cathode. CeO_2-based powders synthesized via the solid state reaction have to be densified by lengthy heating at temperatures as high as 1600–1800 °C to achieve the required chemical homogeneity and desirable densities [7,8]. Such high sintering temperatures leave very little margin for the microstructural control of the resultant ceramics. If dense CeO_2-based electrolytes were able to be prepared at lower temperature, it would be easy to co-sinter them with the electrode material, which would simplify the procedure and lower the costs of fabricating SOFCs. As predicted by Herring's scaling law [9], nanocrystalline powders can provide faster densification kinetics and lower sintering temperatures. Due to the technical importance of CeO_2-based ceramics, several synthetic routes have been developed to produce CeO_2-based powders with nano-sized crystallites, such as the thermal evaporation technique [10] and the wet-chemical process including coprecipitation [11], the hydrothermal process [12], the use of freeze-dried precursors [13] and the combustion technique [14]. However, all of these methods suffer from complexity and

* Corresponding author. Tel.: +82 63 270 2380; fax: +82 63 270 2386.
** Corresponding author. Tel.: +86 27 87863277; fax: +86 27 87864580.
E-mail addresses: kimbh@chonbuk.ac.kr (B.H. Kim), xuqing@whut.edu.cn (Q. Xu).

0272-8842/$34.00
doi:10.1016/j.ceramint.2008.06.014

a low production rate, which limit their applicability. In the past few years, the combustion synthesis of multicomponent ceramic oxides has been gaining reputation as a simple and speedy preparation process to produce homogeneous and fine powders without the need for a calcining step [15,16]. CeO_2-based powders have been successfully synthesized by the combustion technique using different fuels such as glycine [17], carbohydrazide [18] and oxalyldihydrazide [19]. Recently, it was reported that the urea-combustion technique is a suitable route to produce fine and homogenous CeO_2-based powders [20]. However, the study in question only concentrated on the synthesis process and morphology of the powders. No data was provided with regard to the sintering behavior of the powders and electrical performance of the resulting ceramics.

In addition, most of the previous works related to ceria-based solid solutions were concentrated on their electrical conduction properties in air [8,11,17], considering the ceria-based solid solutions as pure oxygen ionic conductors in an oxygen partial pressure, $P_{O_2} > 10^{-5}$ atm, at temperatures, $T < 800\,^{\circ}C$ [21]. However, for application in SOFCs, the solid electrolyte has to directly contact with a reducing fuel, such as H_2 and CO. It has been proven that the reduction of ceria-based solid solutions in a reducing atmosphere significantly deteriorates the output voltage due to mixed ionic-electronic conduction [22,23]. Therefore, it is necessary to ascertain the conditions under which the mixed ionic-electronic conducting behavior starts to appear. Given the above considerations, in the present study, 20 mol% Sm doped CeO_2 ($Ce_{0.8}Sm_{0.2}O_{1.9}$, SDC) ceramics were produced by the urea-combustion technique and their sinterability, microstructure and electrical properties were examined.

2. Experimental

Reagent grade $Ce(NO_3)_3{\cdot}6H_2O$, $Sm(NO_3)_3{\cdot}6H_2O$ and $CO(NH_2)_2$ (urea) were used as starting materials. The nitrates were weighted according to the nominal composition and dissolved into deionized water to form a solution. The amount of urea for the formation of SDC powders can be calculated according to the following equations:

$$8Ce(NO_3)_3{\cdot}6H_2O + 2Sm(NO_3)_3{\cdot}6H_2O + 30CO(NH_2)_2 = 10Ce_{0.8}Sm_{0.2}O_{1.9} + 45N_2 + 30CO_2 + 120H_2O \quad (1)$$

In this case, 1 mol SDC stoichiometrically require 3 mol urea. Therefore, the mole ratio of urea to the total metal cation content was selected as 3.0 in this research. Then, the solution was stirred for 1 h and heated on a hot plate until auto-ignition and self-sustaining combustion occurred. The ash was subsequently ground for 48 h in ethanol medium using a ball milling process with zirconia balls. After the slurry was dried, the as-synthesized powders were uniaxially pressed into disks (10 mm in diameter and 1 mm in thickness) under a pressure of 100 MPa, followed by sintering at 1200–1500 °C for 4 h in air.

Thermogravimetric (TG) analysis and differential scanning calorimetry (DSC) analysis of the as-synthesized powders were preformed using a Netzsch STA449C simultaneous thermal analyzer at a heating rate of $10\,^{\circ}C\,min^{-1}$ in air. The phase composition of the as-synthesized powders was examined by a Rigaku D/MAX-111A X-ray diffractometer using Cu Kα radiation. The morphology of the as-synthesized powders was observed using a Hitachi S-4700 field emission scanning electron microscope (FESEM). For shrinkage behavior study, the as-synthesized powders were compacted into rectangular bars (40 mm × 4 mm × 4 mm) under a pressure of 100 MPa. The linear shrinkage was measured upon heating in air at a heating rate of $10\,^{\circ}C\,min^{-1}$ between 30 and 1500 °C by a Netzsch DIL 402 C dilatometer with alumina as calibration. After thermally etching them, the well-polished surfaces of the ceramic specimens were investigated by means of a Jeol JSM-6400 scanning electron microscope (SEM). The grain sizes were estimated using the linear intercept method with the assistance of image-Pro Plus 6.0 software. The density of the ceramic specimen was measured via the Archimedes method in a water bath and the theoretical density of the SDC was taken as $7.15\,g\,cm^{-3}$ [11].

The AC impedance spectra of these pellets were measured between 350 to 800 °C by an electrochemical workstation (Model IM6e, Zahner, Germany). Measurements were made at intervals of about 50 °C in air and an N_2 + 33.3%H_2 atmosphere over the frequency range of 1 to 3×10^6 Hz. The amplitude of the ac signal imposed on the samples was 50 mV. The sintered pellet was polished to ensure surface flatness and painted with platinum paste. The current collectors were platinum beads and the current leads were platinum wires. The resistance of the leads was subtracted by measuring the impedance of a blank cell.

3. Result and discussion

Fig. 1 shows the TG and DSC curves of the as-synthesized powders. The weight loss of 4.4% from 45 to 700 °C together with a nearly horizontal DSC curve can be observed, suggesting a small amount of organic phase remained in the powders. The phase composition of the as-synthesized powders was studied using the X-ray diffraction (XRD). The resulting diffractogram is indexed and presented in Fig. 2. In accordance with the result of the TG/DSC analyses, all of the characteristic diffraction peaks corresponding to the fluorite cubic structure of CeO_2

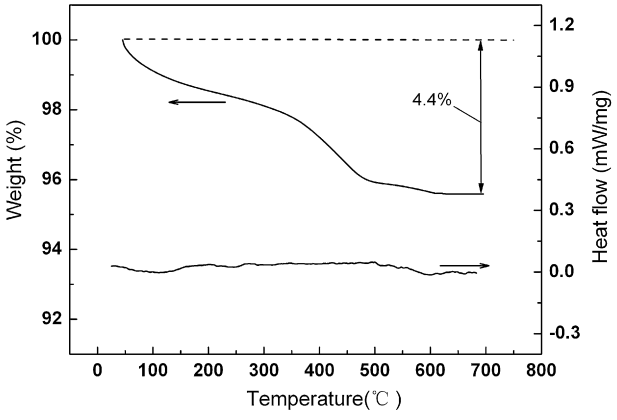

Fig. 1. TG and DSC curves of the as-synthesized powders.

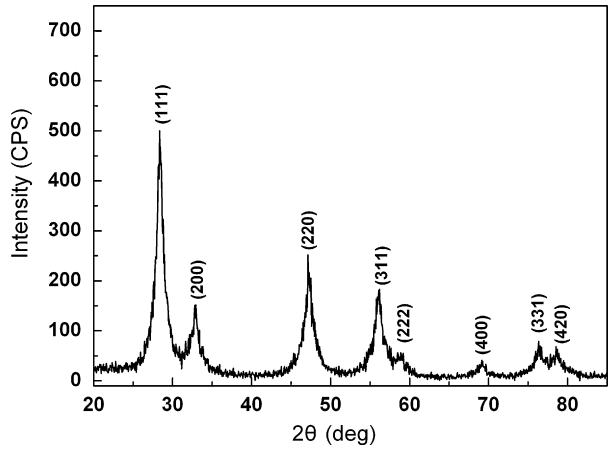

Fig. 2. XRD patterns of the as-synthesized powders.

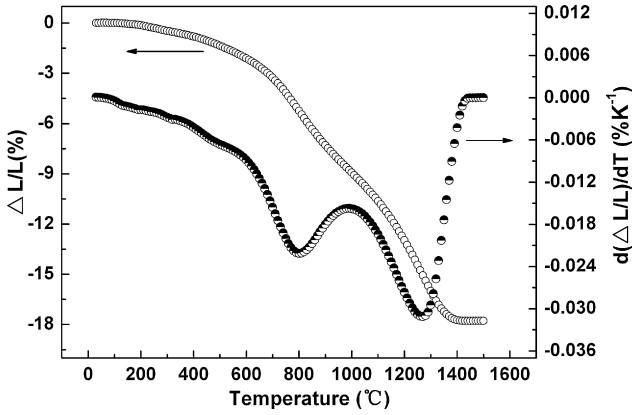

Fig. 4. Linear shrinkage curve of compacted SDC powders.

(JCPDS Card No. 34-394) appeared. No crystalline phase corresponding to Sm_2O_3 could be found, indicating the direct formation of $Ce_{0.8}Sm_{0.2}O_{1.9}$ solid solution without a calcining step. Fig. 3 shows the FESEM micrograph of the as-synthesized powders. It can be seen that the powders consists of homogeneous and fine particles with a diameter of 100–200 nm.

Fig. 4 shows the linear shrinkage behavior of the green compact. Two peaks can be clearly detected in the shrinkage rate curve. One peak corresponding to 800 °C may be ascribe to the formation of neck between the SDC particles during the sintering stage, whereas the other peak around 1250 °C indicates the highest densification rate. Moreover, one can notices the unchanged values of linear shrinkage at temperature above 1400 °C, suggesting the fully densified temperature of the as-synthesized powders. Fig. 5 shows the SEM micrographs of the SDC ceramics sintered at different temperatures. No intragranular pores are observed over the whole sintering temperature range, and all of the pores are located at the grain boundaries or at the triple points. At 1200 °C, the pores exist in the form of continuous open porosity and exhibit a homogenous distribution. After further increasing the sintering temperature, the number and the size of the pores were remarkably reduced. When the sintering temperature is higher than 1350 °C, nearly all of the pores are eliminated from the sintered bodies, and significant grain growth occurs.

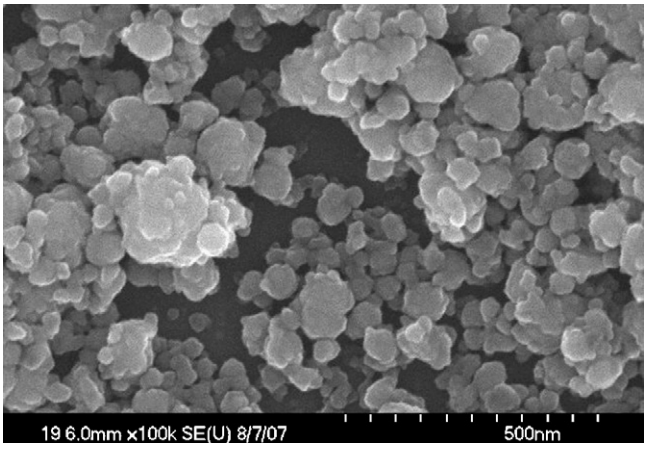

Fig. 3. FESEM micrograph of the as-synthesized powders.

The effect of the sintering temperature on the relative density and grain size of the SDC ceramics are presented in Fig. 6. In the sintering temperature range of 1200–1400 °C, one can see a progressive densification development with increasing sintering temperature in addition to a gradual augment in grain size. By comparison, there is a facilitated grain growth as well as invariance of the relative density in the specimens sintered at above 1400 °C, with the grain size obviously increasing to about 1.5 μm. Those results are generally in agreement with the linear shrinkage behavior of the green compact and microstructural evolution of the SDC ceramics, as shown in Figs. 4 and 5, respectively. Moreover, it should be noted that the SDC powders in this work can be sintered to a relative density of over 95% at a lower sintering temperature of 1250 °C, implying the excellent sinterability of the powders prepared by the urea-combustion technique.

Fig. 7 shows the complex impedance plane plots measured at 350, 450, 500 and 800 °C in air, respectively, of the SDC ceramics sintered at 1350 °C. The impedance characteristics of the SDC ceramics are similar to those of other polycrystalline materials, such as yttria-stabilized zirconia, as well-documented in the literature [24]. At the lower temperature of 350 °C, the grain interior (GI), grain boundary (GB) effects, and electrode polarization behavior (EPB) can be clearly identified from these impedance plots, corresponding to three arcs. However, as the measuring temperature increases, the time constants of the relaxations resulting from the GI and GB effects become short and the arcs shift to higher frequencies, which leads to the successive disappearance of the two corresponding arcs at higher frequencies [8]. The quantitative change of the GI and GB conductivities in the temperature range of 350–450 °C can be obtained by fitting these impedance plots using a software package, while the intercept of the impedance on the $Z' = 0$ axis was employed to determine the total conductivities when the measuring temperatures are higher than 450 °C. The above three kinds of conductivity are considered as macroscopic conductivities, as they are calculated with the macroscopic dimension of the samples

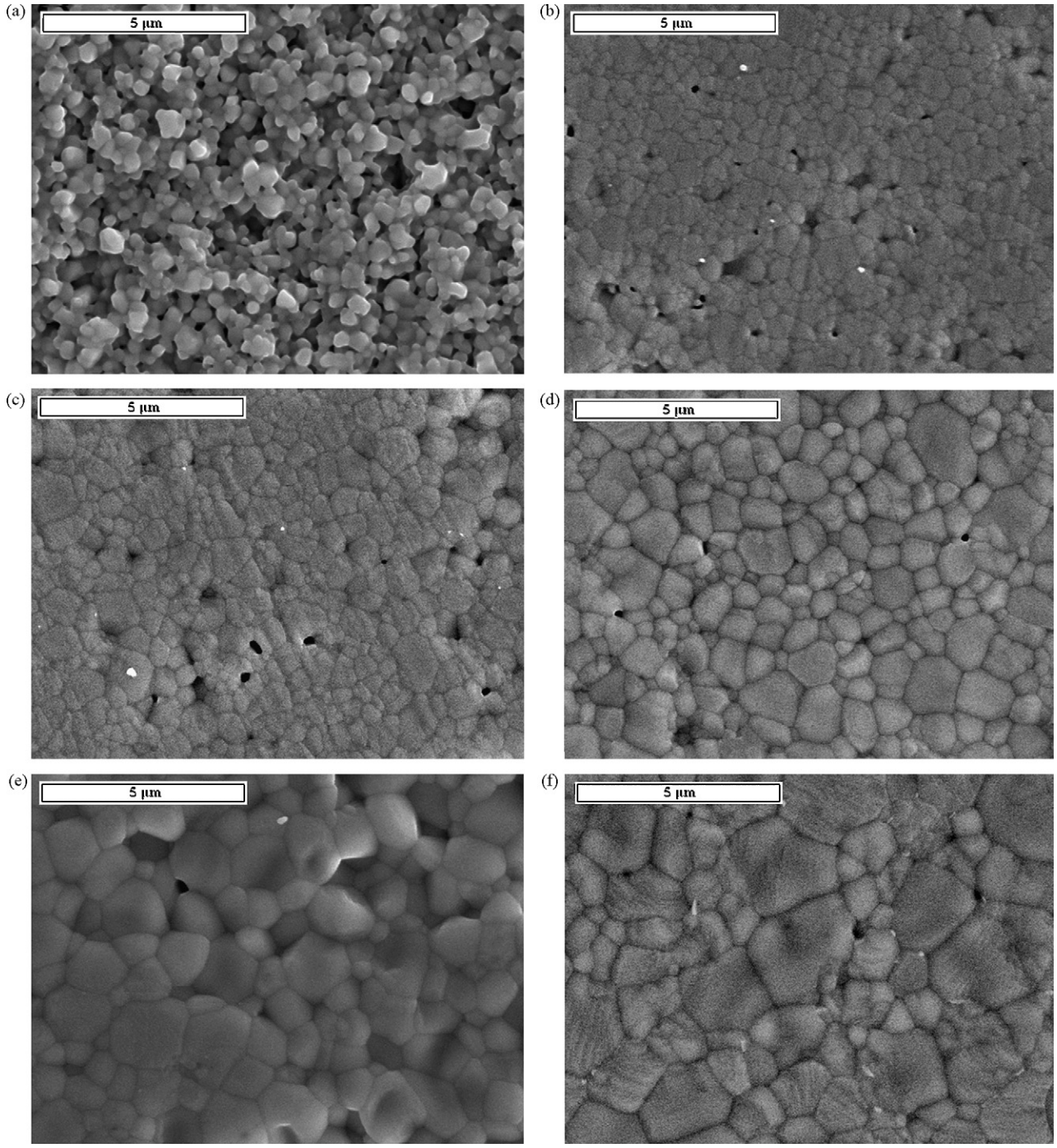

Fig. 5. SEM micrographs of SDC ceramics sintered at (a) 1200 °C, (b)1250 °C, (c)1350 °C, (d)1400 °C, (e)1450 °C, (f)1500 °C.

(thickness/area) [11]. Moreover, the impedance spectra of the ceramic specimens sintered at other temperatures were also resolved using the above method.

The effect of the sintering temperature on the GI ionic conductivity ($\sigma_{ion\ (GI)}$), GB ionic conductivity ($\sigma_{ion\ (GB)}$) and total ionic conductivity ($\sigma_{ion\ (total)}$) of the SDC ceramics measured at 350 °C in air are presented in Fig. 8. The values of $\sigma_{ion\ (GB)}$ and $\sigma_{ion\ (total)}$ display similar changes, increasing with sintering temperature up to a maximum value at 1400 °C and then decreasing. Comparatively, the specimens sintered above 1250 °C present an invariable trend of $\sigma_{ion\ (GI)}$. In Fig. 8, a increase of $\sigma_{ion\ (GI)}$, $\sigma_{ion\ (GB)}$ and $\sigma_{ion\ (total)}$ in the sintering temperature range of 1200–1400 °C can be attributed to the densification of the SDC ceramics. Moreover, when the sintering temperature is higher than 1400 °C, an obvious decrease of $\sigma_{ion\ (GB)}$ can be observed, corresponding to an significant increase of the grain size and invariance of the relative density. It is widely accepted that the relative density and level of impurities are the two major factors responsible for the GB behavior [25]. Compared to grains with a larger size, smaller grain is advantageous to increase the number of grain boundaries in ceramic specimens. These large numbers of grain

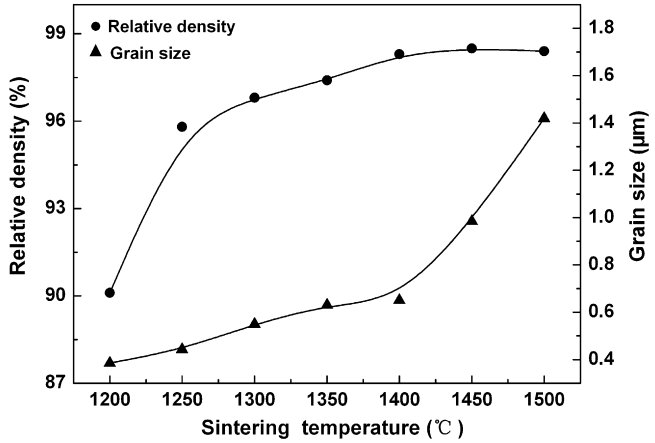

Fig. 6. Relative density and grain size of SDC ceramic as a function of sintering temperature.

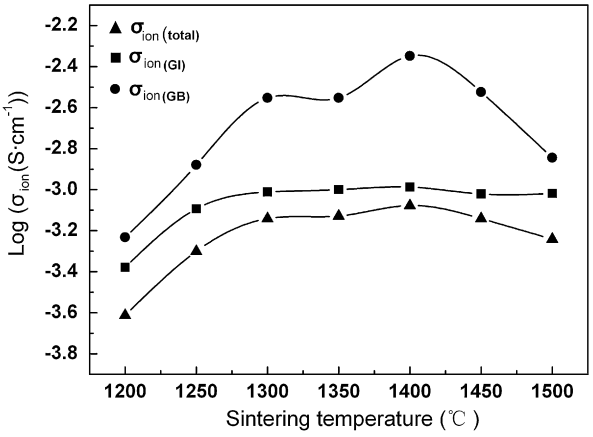

Fig. 8. $\sigma_{ion\ (GI)}$, $\sigma_{ion\ (GB)}$ and $\sigma_{ion\ (total)}$ of SDC ceramics measured at 350 °C in air, as a function of sintering temperature.

boundaries allow the impurities to be dispersed to a large extent and cause the amount of impurities located in the grain boundaries to be reduced, thereby facilitating the movement of oxygen vacancies across the grain boundaries. Considering their identical relative densities and similar $\sigma_{ion\ (GI)}$ values over the sintering temperature range of 1400–1500 °C, the grain size of the SDC ceramics play a decisive role in determining the values of $\sigma_{ion\ (GB)}$ and $\sigma_{ion\ (total)}$ at a measuring temperature of 350 °C. On the basis of this analysis, we can conclude that keeping the grain size small in the process of fabricating dense

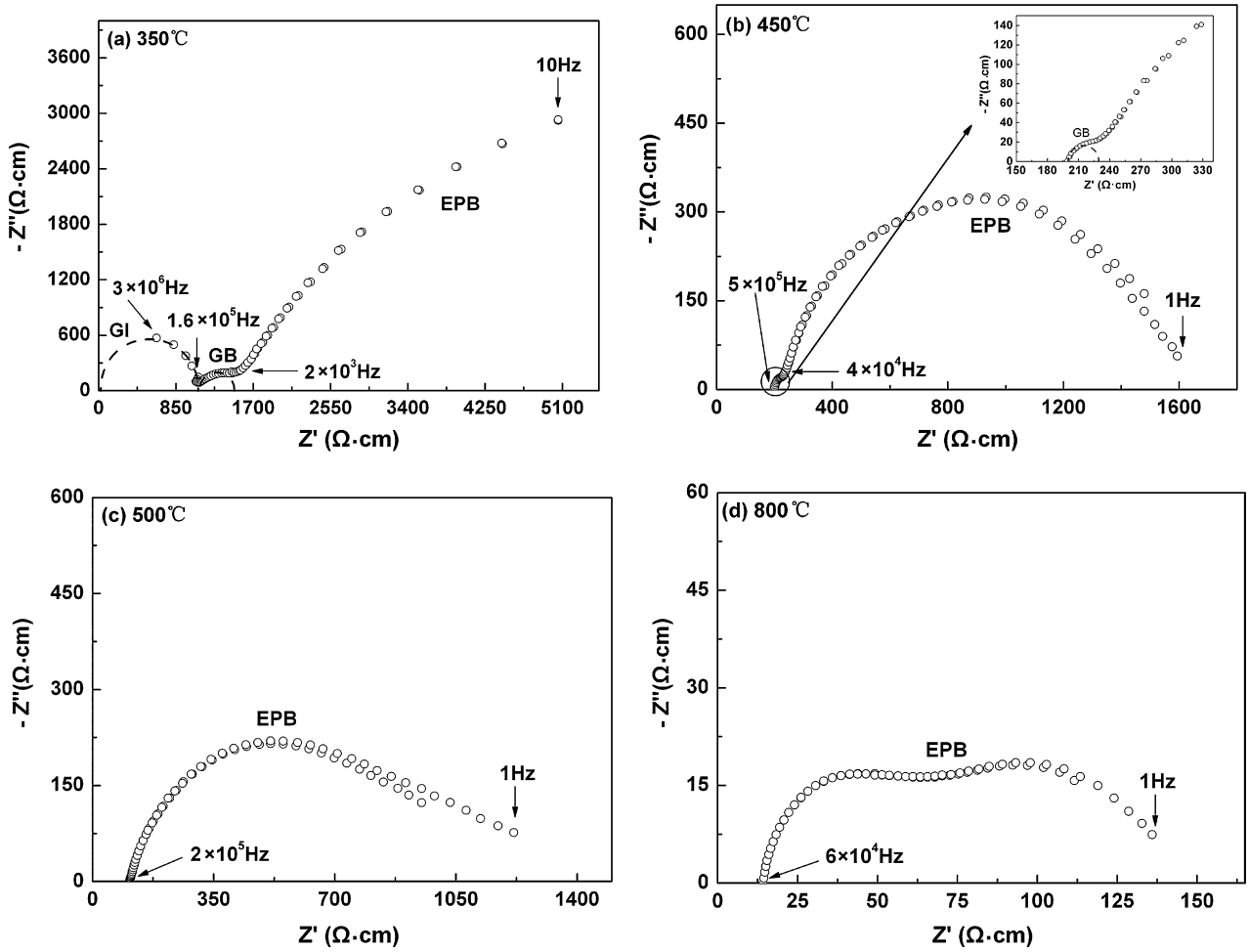

Fig. 7. Impedance plots of SDC ceramic sintered at 1350 °C, measured at (a) 350 °C, (b) 450 °C, (c) 500 °C and (d) 800 °C in air. The GI, GB and EPB stand for grain interior, grain boundary effects, and electrode polarization behavior, respectively. For the sake of clarity, the fitting results of the electrode polarization behavior are not presented.

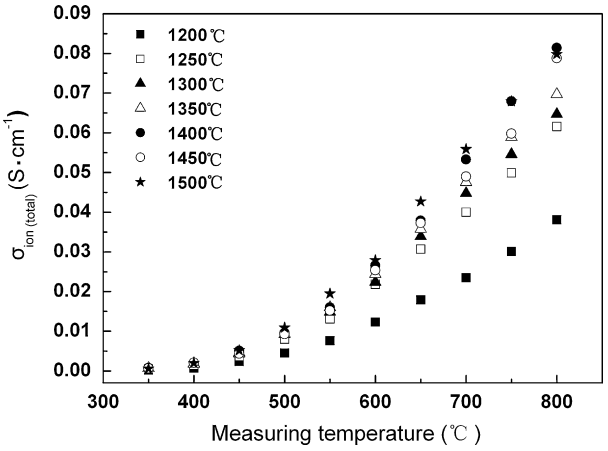

Fig. 9. Temperature dependence of $\sigma_{ion\ (total)}$ for SDC ceramics sintered at different temperatures (Measurement in air).

SDC ceramics is beneficial to enhance the ionic conductivity at lower temperatures.

Fig. 9 shows the $\sigma_{ion\ (total)}$ values of the SDC ceramics in air as a function of the measuring temperature. The $\sigma_{ion\ (total)}$ values of the specimens sintered at different temperatures display a monotonous increase with measuring temperature. Such a variation in ionic conduction originated from the transference of oxygen vacancy is similar to the previously reported results [11,17]. In the case of the same measuring temperature, the $\sigma_{ion\ (total)}$ value increases with sintering temperature and attains the largest values at 1400 °C, followed by an invariability of $\sigma_{ion\ (total)}$ with further elevated sintering temperature. The specimens sintered from 1400 to 1500 °C offer a maximum $\sigma_{ion\ (total)}$ value of around 0.081 S cm^{-1} at 800 °C, which is comparatively similar to the literature value of ~0.082 S cm^{-1} obtained from specimens made by the glycine-nitrate process [17]. At intermediate temperatures (600–800 °C), the specimens gives ionic conductivities of 0.026–0.081 S cm^{-1}, roughly near to the ionic conductivity requirement for the electrolyte materials of SOFCs.

Fig. 10 shows the Arrhenius plots of σ_{ion} (total) for SDC ceramics sintered at different temperatures. The insets display the Arrhenius plots of $\sigma_{ion\ (GI)}$ and $\sigma_{ion\ (GB)}$ in the lower temperature range. It can be seen that the Arrhenius curve of $\sigma_{ion\ (total)}$ cannot be fitted by a single straight line. There exists a pronounced curvature near 560 °C for all of the ceramic specimens, which divides the Arrhenius curve into two regions. This result is generally in accordance with the previous research conducted by Kliner and Walters [26]. At elevated temperatures, the electrical conduction is controlled by the population of charge-carrying defects determined by an aliovalent (Sm).

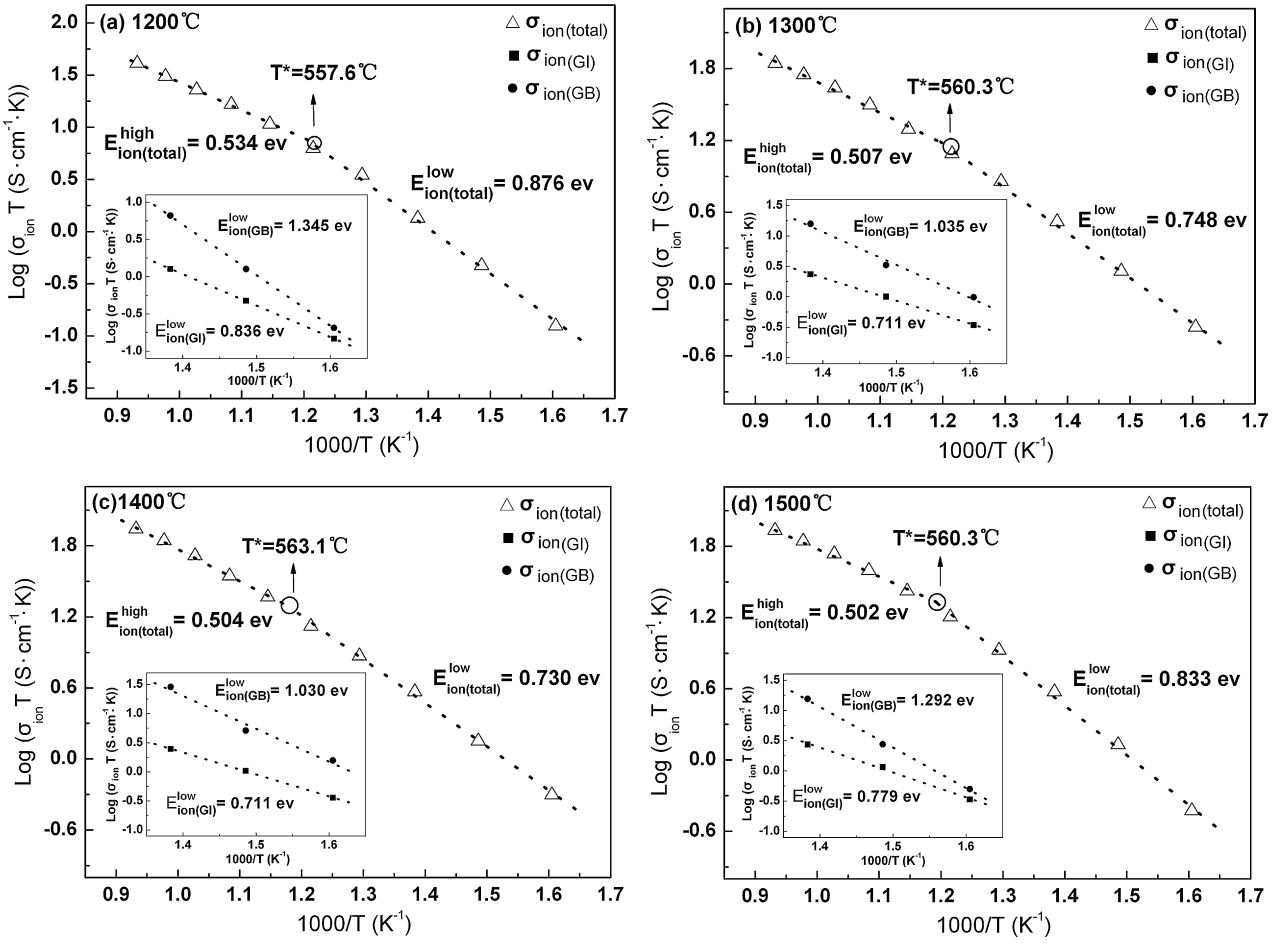

Fig. 10. Arrhenius plots of $\sigma_{ion\ (total)}$ for SDC ceramics sintered at different temperatures. The insets show the Arrhenius plots of $\sigma_{ion\ (GI)}$ and $\sigma_{ion\ (GB)}$) in the lower temperature range (Measurement in air).

At lower temperatures, the population of charge-carrying defects is determined by the thermodynamic equilibrium between the free defects and the associated pairs (Sm'_{Ce}-$V_O^{\bullet\bullet}$). Thus, the slope of the line becomes sharper due to the large activation energy of electrical conduction. However, for the value of $\sigma_{ion\ (GI)}$ and $\sigma_{ion\ (GB)}$, we can only obtain the effective data in the temperature range of 350–450 °C due to the limitation of AC Impedance spectra, as described in Fig. 7. The Activation energies named as $E^{high}_{ion(total)}$, $E^{low}_{ion(total)}$, $E^{low}_{ion(GI)}$ and $E^{low}_{ion(GB)}$, corresponding to the $\sigma_{ion\ (total)}$ in the high temperature range, $\sigma_{ion\ (total)}$ in the low temperature range, $\sigma_{ion\ (GI)}$ in the low temperature range and $\sigma_{ion\ (GB)}$ in the low temperature range of the SDC ceramics sintered at different temperatures (measurement in air) are calculated from the linear fit of the Arrhenius plots and displayed in Fig. 11. It can be found that the $E^{high}_{ion(total)}$ value declines monotonously with increasing sintering temperature, corresponding to the variation of $\sigma_{ion\ (total)}$ in the higher temperature range as a function of the sintering temperature. Moreover, the values of $E^{low}_{ion(total)}$, $E^{low}_{ion(GI)}$ and $E^{low}_{ion(GB)}$ display an identical variation accordingly, decreasing with the sintering temperature to a minimum value and then increasing above 1400 °C. The enhancement of $E^{low}_{ion(GB)}$ starting from 1400 °C may be ascribed to significant grain growth over the same sintering temperature range, resulting in a decrease of $\sigma_{ion\ (total)}$ at lower measuring temperatures, as illustrated in Fig. 8.

Fig. 12 shows the impedance plots of the SDC ceramic sintered at 1450 °C, measured at 500 °C in air and an $N_2 + 33.3\%H_2$ atmosphere. As described in Fig. 7, the contribution of GI and GB to the impedance spectra becomes indistinguishable, when the measuring temperature is higher than 450 °C. Consequently, the impedance plots in Fig. 12 can be ascribed to the effect of the EPB alone. Compared to the impedance spectra recorded in air, the impedance plots

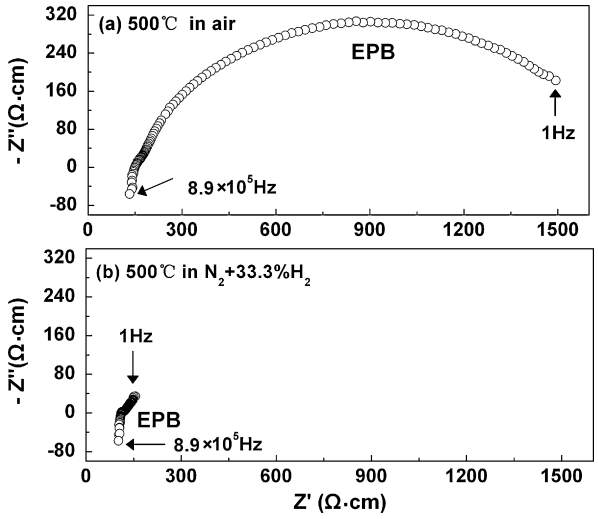

Fig. 12. Impedance plots of SDC ceramic sintered at 1450 °C, measured at 500 °C in (a) air and (b) $N_2 + 33.3\%H_2$ atmosphere.

measured in $N_2 + 33.3\%H_2$ over the same frequency range from 1 Hz to 8.9×10^5 Hz become concentrated in a remarkable way, leading to an insignificant plot for the EPB. This phenomenon was also reported by Huang et al. in the case of $Ce_{0.9}Gd_{0.1}O_{1.95}$ ceramics, who considered the concentrated impedance plots in the $Ar + 10\%H_2$ atmosphere as a pronounced Warburg feature [21]. In order to provide more support for the above explanation, we chose to analyze some characteristics of the Warburg impedance in a more qualitative way.

Fig. 13 shows the impedance (Z) of the SDC ceramic sintered at 1450 °C as a function of $1/\omega^{1/2}$ ($\omega = 2\pi f$, where f represents the value of the frequency), measured at 500 °C in air and an $N_2 + 33.3\%H_2$ atmosphere. The inset in Fig. 13(b)

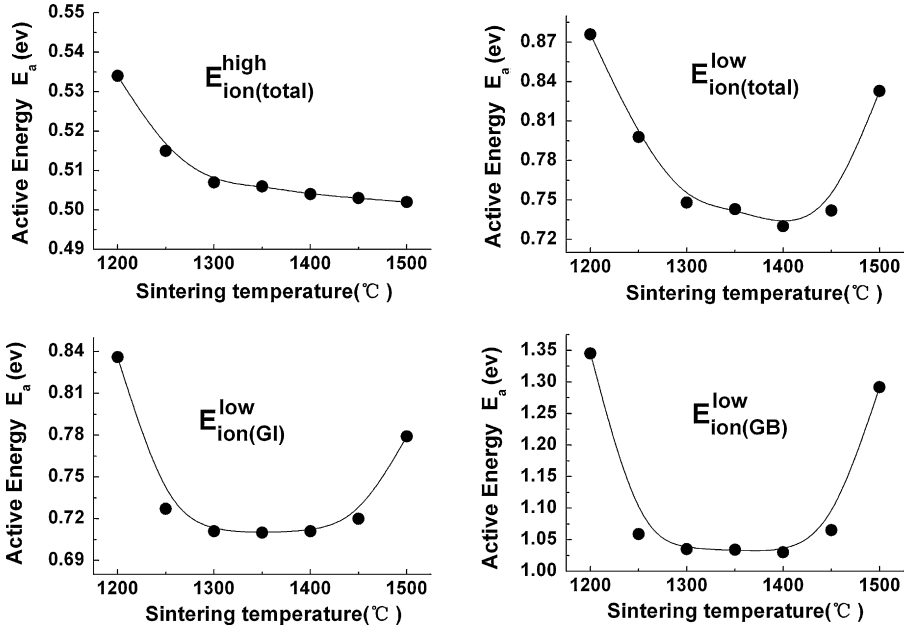

Fig. 11. The Activation energies named as $E^{high}_{ion(total)}$, $E^{low}_{ion(total)}$, $E^{low}_{ion(GI)}$ and $E^{low}_{ion(GB)}$ of the SDC ceramics sintered at different temperatures (Measurement in air).

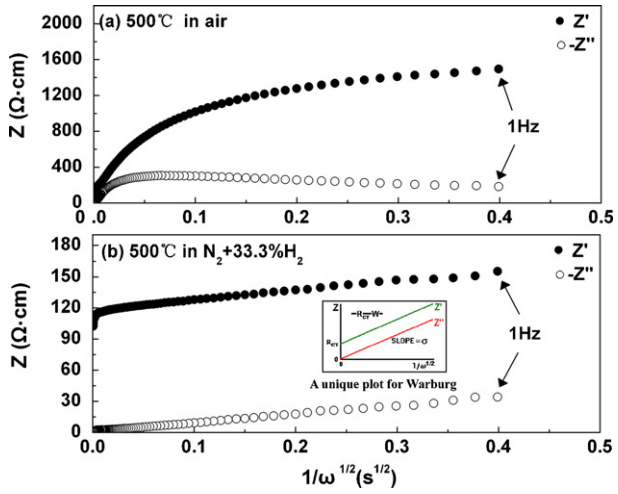

Fig. 13. Impedance (Z) of SDC ceramic sintered at 1450 °C as a function of $1/\omega^{1/2}$ ($\omega=2\pi f$, where f represents the value of the frequency), measured at 500 °C in (a) air and (b) $N_2 + 33.3\%H_2$ atmosphere. The inset in Fig. 12(b) shows a unique plot for the Warburg impedance [29].

shows a unique plot for the Warburg impedance. Both the real and imaginary parts of Z are plotted vs. $1/\omega^{1/2}$. The lines should be straight and parallel. The slope of both lines should be equal to the Warburg constant. The line for the imaginary component (Z'') should intersect the Z axis at zero, while the intercept for the real component (shown in green) is R_{CT} [27]. It can be observed from Fig. 13(a) that there exist two curves corresponding to the variations of Z' and $-Z''$, respectively. Comparatively, the two parallel straight lines in Fig. 13(b) imply a typical Warburg feature of the EPB contribution, indicating that the interfacial diffusion of oxygen atoms dominates the impedance in reducing atmosphere with the lowest O_2 partial pressure [21].

In Fig. 12, the left intercept of the impedance on the $Z' = 0$ axis can also be utilized to determine the total electrical conductivities (σ_{total}) in air and the $N_2 + 33.3\%H_2$ atmosphere, and the value of σ_{total} at other measuring temperatures can be acquired using the method illustrated in Fig. 7. Fig. 14 shows the σ_{total} value of the SDC ceramic sintered at 1450 °C as a function of the measuring temperature, measured in air and the $N_2 + 33.3\%H_2$ atmosphere. In the measuring temperature range of 350–550 °C, the plots representing the σ_{total} value in the two atmospheres overlap each other. However, from 600 °C, the σ_{total} value in the $N_2 + 33.3\%H_2$ atmosphere increases sharply, followed by an enhancement of the differences between the σ_{total} values in the two atmospheres. These changes are due to the introduction of a mixed Ce^{4+}/Ce^{3+} valence state and generation of the electronic conduction in reducing atmosphere. Therefore, for its application in an SOFC, the SDC electrolyte should be operated at temperatures below 600 °C to avoid the loss of efficiency. Based on the above considerations, the $\sigma_{ion\ (total)}$ value at 550 °C should be considered as a crucial parameter to evaluate the performance of ceria-based solid electrolytes. In Fig. 9, the specimen sintered from 1400 to 1500 °C offer a maximum $\sigma_{ion\ (total)}$ value of around 0.019 S cm^{-1} at 550 °C, which is almost three times larger than the literature values of ~0.005 S cm^{-1} and 0.006 S cm^{-1} at 600 °C obtained from the specimens made by sol-gel method [28] and hydrothermal process [29], respectively, demonstrating the advantage of the urea-combustion technique in preparing the SDC solid electrolyte.

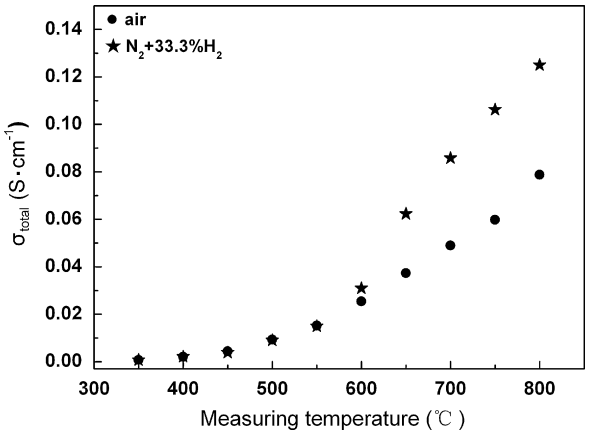

Fig. 14. Total conductivity (σ_{total}) of SDC ceramic sintered at 1450 °C as a function of measuring temperature, measured in air and $N_2 + 33.3\%H_2$ atmosphere.

4. Conclusions

The urea-combustion technique was shown to be an advantageous and efficient route to producing SDC ceramics. The fine powders synthesized by the urea-combustion technique can be sintered to a relative density of over 95% at a lower sintering temperature of 1250 °C, implying the excellent sinterability of the powders. It was found that the density and microstructure evolution are responsible for the variation in the electrical conducting properties with the sintering temperature. Keeping the grain size small during the process of fabricating dense SDC ceramics is beneficial to enhance the ionic conductivity at lower temperature. The specimens sintered at temperatures above 1350 °C exhibit an excellent total ionic conductivity of 0.082 S cm^{-1} at 800 °C in air. However, when measuring in an $N_2 + 33.3\%H_2$ atmosphere, a pronounced Warburg feature appears in the impedance plots of the SDC ceramics, together with a significant increase of the total conductivity above the measuring temperature of 550 °C, due to the introduction of a mixed Ce^{4+}/Ce^{3+} valence state and the generation of the electronic conduction in the reducing atmosphere. The total conductivity at 550 °C should be considered as a crucial parameter to evaluate the performance of ceria-based solid electrolytes.

Acknowledgements

This work was financially supported by the International Collaboration Program of Jeonbuk Province and Korea Research Foundation Grant funded by the Korean Government (MOEHRD, KRF-2007-211-D00053). The authors are also thankful to the Natural Science Foundation of China (Grant No. 50572079) for supporting the research.

References

[1] D.Y. Wang, D.S. Park, J. Griffith, A.S. Nowick, Oxygen-ion conductivity and defect interactions in yttria-doped ceria, Solid State Ionics 2 (1981) 95–105.

[2] G.B. Balazs, R.S. Glass, AC impedance studies of rare earth oxide doped ceria, Solid State Ionics 76 (1995) 155–162.

[3] C. Tian, S.W. Chan, Ionic conductivities, sintering temperatures and microstructures of bulk ceramic CeO_2 doped with Y_2O_3, Solid State Ionics 134 (2000) 89–102.

[4] T.S. Zhang, P. Hing, H.T. Huang, J.A. Kilner, Ionic conductivity in the CeO_2–Gd_2O_3 system ($0.05 \leq Gd/Ce \leq 0.4$) prepared by oxalate coprecipitation, Solid State Ionics 148 (2002) 567–573.

[5] R. Gerhard-Anderson, A.S. Nowick, Ionic conductivity of CeO_2 with trivalent dopants of different ionic radii, Solid State Ionics 5 (1981) 547–550.

[6] J.A. Kilner, Fast anion transport in solids, Solid State Ionics 8 (1983) 201–207.

[7] T. Kuto, H. Obayashi, Oxygen Ion conduction of the fluorite-Type $Ce_{1-x}Ln_xO_{2-x/2}$ (Ln = Lanthanoid Element), J. Electrochem. Soc. 122 (1975) 142–147.

[8] Z.L. Zhan, T.L. Wen, H.Y. Tu, Z.Y. Lu, AC impedance investigation of Samarium-doped ceria, J. Electrochem. Soc. 148 (2001) A427–A432.

[9] P. Klug, L.E. Alexander, Diffraction Procedure for Polycrystalline and Amorphous Materials, Wiley, New York, 1954, 188.

[10] W. Bai, K.L. Choy, N.H.J. Stelzer, J. Schoonman, Thermophoresis-assisted vapour phase synthesis of CeO_2 and $Ce_xY_{1-x}O_{2-\delta}$ nanoparticles, Solid State Ionics 116 (1999) 225–228.

[11] H.B. Li, C.R. Xia, M.H. Zhu, Z.X. Zhou, G.Y. Meng, Reactive $Ce_{0.8}Sm_{0.2}O_{1.9}$ powder synthesized by carbonate coprecipitation: sintering and electrical characteristics, Acta. Mater. 54 (2006) 721–727.

[12] J.S. Lee, S.C. Choi, Crystallization behavior of nano-ceria powders by hydrothermal synthesis using a mixture of H_2O_2 and NH_4OH, Mater. Lett. 58 (2004) 390–393.

[13] D. Perez-coll, P. Nunez, J.R. Frade, J.C.C.C. Abrantes, Conductivity of CGO and CSO ceramics obtained from freeze-dried precursors, Electrochimica Acta 48 (2003) 1551–1557.

[14] C.C. Hwang, T.H. Huang, J.S. Tsai, C.S. Lin, C.H. Peng, Mat. Sci. Eng. B 132 (2006) 229–238.

[15] D.A. Fumo, M.R. Morelli, A.M. Segadaes, Combustion synthesis of calcium aluminates, Mater. Res. Bull. 31 (1996) 1255.

[16] M.T. Colomer, D.A. Fumo, J.R. Jurado, A.M. Segadaes, Non-stoichiometric $La_{(1-x)}NiO_{(3-\delta)}$ perovskites produced by combustion synthesis, J. Mater. Chem. 9 (1999) 2505–2510.

[17] R.R. Peng, C.G. Xia, Q.X. Fu, G.Y. Meng, D.K. Peng, Sintering and electrical properties of $(CeO_2)_{0.8}(Sm_2O_3)_{0.1}$ powders prepared by glycine–nitrate process, Mater. Lett. 56 (2002) 1043–1047.

[18] S.T. Aruna, S. Ghosh, K.C. Patil, Combustion synthesis and properties of $Ce_{1-x}Pr_xO_{2-\delta}$ red ceramic pigments, Int. J. Inor. Mater. 3 (2001) 387–392.

[19] S.T. Aruna, K.C. Patil, Combustion synthesis and properties of nanostructured ceria-zirconia solid solutions, Nanostruct. Mater. 10 (1998) 955–964.

[20] E. Chinarro, J.R. Jurado, M.T. Colomer, Synthesis of ceria-based electrolyte nanometric powders by urea-combustion technique, J. Eur. Ceram. Soc. 27 (2007) 3619–3623.

[21] K.Q. Huang, M. Feng, J.B. Goodenough, Synthesis and electrical properties of dense $Ce_{0.9}Gd_{0.1}O_{1.95}$ ceramics, J. Am. Ceram. Soc. 81 (1998) 357–362.

[22] T. Kuto, H. Obayashi, Mixed Electrical Conduction in the Fluorite-Type $Ce_{1-x}Gd_xO_{2-x/2}$, J. Electrochem. Soc. 123 (1976) 415–419.

[23] K. Eguchi, T. Setoguchi, T. Inoue, H. Arai, Electrical properties of ceria-based oxides and their application to solid oxide fuel cells, Solid State Ionics 52 (1992) 165–172.

[24] J.E. Bauerle, Study of solid electrolyte polarization by a complex admittance method, J. Phys. Chem. Solids 30 (1969) 2657–2670.

[25] J. Ma, T.S. Zhang, L.B. Kong, P. Hing, S.H. Chan, $Ce_{0.8}Gd_{0.2}O_{2-\delta}$ ceramics derived from commercial submicron-sized CeO_2 and Gd_2O_3 powders for use as electrolytes in solid oxide fuel cells, J. Power Source 132 (2004) 71–76.

[26] J.A. Kliner, C.D. Walters, The effects of dopant cation-oxygen vacancy complexes on the anion transport properties of non-stoichiometric fluorite oxides, Solid State Ionics 6 (1982) 253–259.

[27] A.J. Bard, L.R. Faulkner, Electrochemical methods: fundamentals and applications, John Wiley and Sons, New York, 2001.

[28] W. Huang, P. Shuk, M. GreenBlatt, Properties of sol-gel prepared $Ce_{1-x}Sm_xO_{2-x/2}$ solid electrolytes, Solid State Ionics 100 (1997) 23–27.

[29] W. Huang, K.P. Shu, M. Greenblatt, Hydrothermal synthesis and properties of $Ce_{1-x}Sm_xO_{2-x/2}$ and $Ce_{1-x}Ca_xO_{2-x}$ solid solutions, Chem. Mater 9 (1997) 2240–2245.